Proceedings of the 4th ACPMG 2024
4th Asia-Pacific Conference on Physical Modelling in Geotechnics
11-13 December 2024, Abu Dhabi, UAE

Validation of a countermeasure against pipe uplift during liquefaction

H.K. Hong
Kansai University, Suita, Japan, k561984@kansai-u.ac.jp

T. Tobita
Kansai University, Suita, Japan, tobita@kansai-u.ac.jp

K. Miyamoto, Y. Konishi
Nihon Suido Consultants Co., Ltd., Suita, Japan, miyamoto_k@nissuicon.co.jp, konisi_y@nissuicon.co.jp

ABSTRACT: This study aims to find countermeasures to mitigate buried pipe uplift damage in earthquake-induced liquefied ground. By examining the effects of various countermeasures through centrifuge experiments and numerical analyses, considerations for countermeasure design were identified. The countermeasures using high-permeable materials in existing studies were judged to overlap with the other effects, so the effectiveness of pure high-permeable materials was investigated through centrifuge experiments and numerical analysis. Replacing the upper-side soil with high-permeable soil can reduce EPWP. However, it was found that the high-permeable material may generate pipe uplift-prone pressure conditions, which induce more uplift. In addition, a countermeasure using a horizontal plate designed by removing factors that promote pipe uplift, as mentioned in existing studies, was verified through numerical analysis. Using horizontal plates as a countermeasure is an effective way to mitigate pipe uplift by reducing the EPWP ratio around the pipe and increasing resisting soil volume against pipe uplift.

1 INTRODUCTION

Underground pipes play a vital role in transporting water and sewage. However, during an earthquake, liquefaction may occur due to the excess pore water pressure (EPWP) build-up. Then, the soil behaves like a liquid and generates a buoyancy force that uplifts underground pipes, which may cause severe damage to sewage and water supply systems.

Previous studies provided that burial conditions, seismic load characteristics, and soil properties determine pipe uplift vulnerability. The pipe uplift is prone when the ratio of pipe burial depth (H) to pipe diameter (D) (H/D) is low. This is because the burial depth is a significant portion of the uplift resistance by the upper soil, and the pipe diameter is proportional to the buoyancy force generated by the density difference between the liquefied soil and the pipe (Chian et al., 2012; Chian et al., 2014; Sharafi et al., 2016). Also, it has been studied that seismic load characteristics determine pipe uplift behaviour. The pipe uplift is susceptible to increases in peak ground acceleration, significant duration, and Arias intensity (Basu et al., 2024). The influence of soil properties is known to be significant. Pipes are susceptible to uplift when the relative density and soil friction angle are low, and the dilatancy angle is large (Sharafi et al., 2016).

Existing studies have proposed various types of countermeasures. Methods of reducing pipe uplift by dissipating EPWP have been proposed. The high-permeable gravel bag drastically reduces pipe uplift (Castiglia et al., 2021), and the sand-rubber mixture reduces uplift (Valizadeh et al., 2022; Ecemis et al., 2021). Placing drainpipes around the pipe is also a method of mitigating the EPWP build-up (Castiglia et al., 2021). Methods of applying a rigid weight structure heavier than soil to the pipe's upper side were analysed. However, it was mentioned that even though the countermeasure has a heavier density than soil, there are cases where a larger uplift occurs. This is because the rigid structure's dynamic inertia force-induced shear deformation during shaking increases the surrounding soil's EPWP (Hong et al., 2024). A steel bar and plate structure called a horn-type structure at the pipe's top was proposed; the non-liquefied layer supports the pipe (Taeseri et al., 2016). Geogrid was also used by placing on the pipe's upper soil, reducing the uplift due to the shear deformation suppression (Castiglia et al., 2021).

However, the cases of mitigated uplift in previous studies have possibilities due to the combined effect. The possibility of constraining deformation due to the gravel bag's "bag" and the soil's physical properties

changing due to the sand-rubber mixture overlaps with the effects of the high-permeable material. Also, the tested conditions of some previous studies are far from the pipe uplift-prone conditions, such as deep burial depth and low groundwater level.

Furthermore, the characteristic of inducing more EPWP during shaking of the structure countermeasure provides that the countermeasure should avoid the shape of vertically facing the surrounding soil, which means that horizontal plate type should be considered.

Therefore, this study tries to verify the pure effect of the high-permeable material countermeasure through experiment and numerical analysis. It also investigates the horizontal plate countermeasures effects with numerical analysis. The experiments and numerical analyses are conducted under fully saturated and shallow-buried conditions, which are vulnerable conditions to uplift.

2 CENTRIFUGE MODELING

Due to the nonlinear stress-strain relationship of soil, experiments on soil with stress conditions of 1/*N* model size may show differences with prototype-scale ground. Geotechnical centrifuge modelling has been used to experiment in prototype stress conditions, achieved by centrifugal acceleration of *N*×g level (Madabhushi, 2017). This study used the centrifuge at Kansai University, Japan, under 50g conditions. A rigid box was used as the model container.

Figure 1 shows the schematic view of the model on a prototype scale. The soil used in the experiment was Toyoura sand, shown in Table 1. The high-permeable countermeasure material is Silica No.3, which has 3.6×10^{-3}m/s of higher permeability coefficient (*k*) (Ueno et al., 2017; Asano et al., 2010) than Toyoura sand (2×10^{-4}m/s) (Mori et al., 1986; Inoue et al., 2019). It is named crushed stone countermeasure (CSC). The pipes are 9m long, 2.5m in diameter (*D*), 0.2g/cm^3 density, and burial depth (*H*) is 2.5m on the prototype scale, which is the condition of *H*/*D* equals to 1. The model ground was modelled by air pluviation. The ground relative density was measured at 58.1% after consolidation under 50g. The water level was kept higher (1.5m) than the ground surface to maintain the fully saturated condition. The input motion is a ramped sine wave, as shown in Figure 2.

Table 1. Toyoura sand material properties (laboratory test).

Properties	Value
Specific gravity G_s	2.66
Minimum void ratio e_{min}	0.62
Maximum void ratio e_{max}	0.94
Maximum dry density ρ_{max} (kg/m^3)	1640.77
Minimum dry density ρ_{min} (kg/m^3)	1371.12

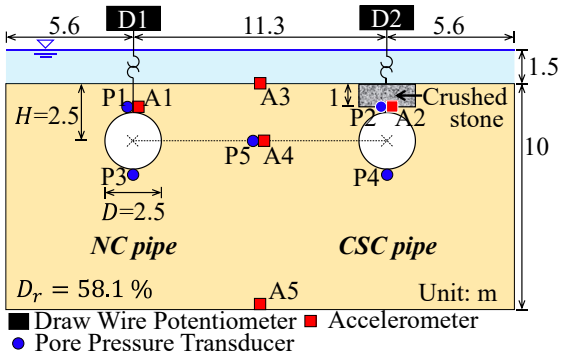

Figure 1. Experiment model (Prototype scale).

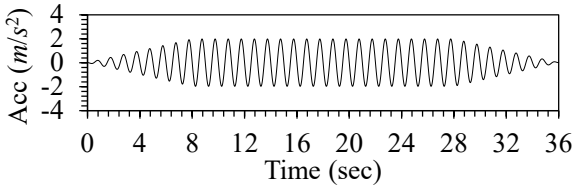

Figure 2. Input motion (Prototype scale).

3 NUMERICAL MODELING

The FLIP ROSE ver.7.4.3 (Finite element analysis program of liquefaction process/Response of soil-structure systems during earthquakes) is used for the numerical analysis (Iai et al., 2011). The soil element is modelled using a Cocktail glass model, which represents the strain space multiple shear mechanisms and incorporates a stress-dilatancy relationship, where the dilatancy is the sum of the contractive and dilative parts based on the void ratio (Iai et al., 2011). Table 2 shows the calibrated input parameters of Toyoura sand in 58.1% of relative density based on the existing study's interpolated experimental results (Asadi et al., 2019). Figure 3 shows the liquefaction resistance curve in Table 2 and the existing study.

Table 2. Input parameters of soil model.

	Parameter designation	Value
G_{ma}	Shear modulus (kPa)	78401
K_{L/U_a}	Bulk modulus (kPa)	204461
ρ_t	Mass density (t/m^3)	1.95
n	Porosity	0.43
ϕ_f^{PS}	Internal friction angle (°)	41
ϕ_P	Phase transformation angle (°)	28
ε_d^{cm}	Limit of contractive component	0.15
$r_{\varepsilon_d^c}$	$(-)$ dilatancy control parameter	3.0
r_{ε_d}	$(+)/(-)$ dilatancy parameter	0.2
q_1	EPWP initial phase control parameter	3.0
q_2	EPWP final phase control parameter	0.75
r_k	K_{L/U_a} reduction factor	0.3
c_1	Parameter controlling lower limit of liquefaction resistance curve	1.5

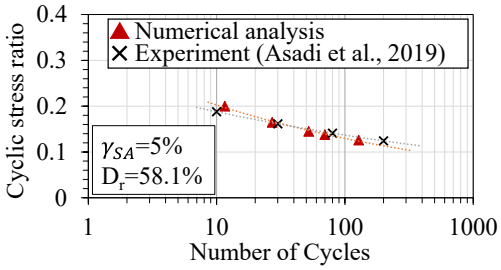

Figure 3. Liquefaction resistance curve of Toyoura sand.

Figure 4 shows the numerical modelling and boundary conditions. The water above the ground surface did not affect the numerical analysis, so the groundwater level was set to the ground surface. A single pipe model was used in each numerical analysis case. The boundary conditions are the same as the rigid box in the experiment: the bottom is fixed, and both sides are fixed for the lateral and free for the vertical

Figure 4 (a), (b), (c), and (d) are the numerical modelling of the homogeneous soil, NC pipe, CSC pipe, and DSC (dango shape countermeasure) pipe models, respectively. The differences between homogeneous soil and NC pipe models represent the pure effects of the pipe. This analysis will provide the liquefaction behaviour during pipe uplift, which shows the considerations of countermeasure design against pipe uplift. CSC is modelled the same as the ground model except for permeability to investigate the pure effect of the high-permeable countermeasure. DSC is the horizontal plate countermeasure. The horizontal plate effect may differ depending on the placement (e.g. top or bottom). However, the horizontal plate was applied at the mid-height of the pipe to evaluate the applicability of the horizontal plate countermeasure in this study. It is named for its cross-sectional shape, similar to the "dango," a traditional Japanese food. The effects of the CSC and DSC are demonstrated by comparing them with the NC pipe model.

The pipe and DSC are modelled linear plane models with densities of 0.2 g/cm^3 and 1.95 g/cm^3, respectively. The density of DSC (1.95 g/cm^3) is equal to the soil density, which is not affected by buoyancy. The input motion is equal to the experiment (Figure 2).

Table 3 shows numerical analysis cases. Liquefaction behaviour under seismic loading can be categorized as drained and undrained conditions. Drained conditions consider soil permeability, which allows pore water movement; undrained conditions do not. According to Zienkiewicz et al. (1980), the seismic load is instantaneous, and the soil permeability is small; undrained conditions are known to be well-matched. However, the CSC case is on the effect of different permeability materials, which the drained condition should apply. Therefore, this study conducted numerical analyses under drained conditions for CSC and under undrained conditions for DSC. Homogeneous and NC pipe models are simulated under both as a comparison group.

CSC 1 is conducted to validate the experiment. CSC 2 and CSC 3 are the cases that analyse the pipe uplift trend according to the CSC's permeability. CSC 2 and CSC 3 cases are selected conditions without divergence caused by a large permeability difference from the ground model. DSC 1 to DSC 5 is used to analyse the pipe uplift trend with increasing horizontal plate length. The length of the horizontal plate is normalized to the ratio of the single horizontal plate length (L) and the pipe diameter (D) in Figure 4.

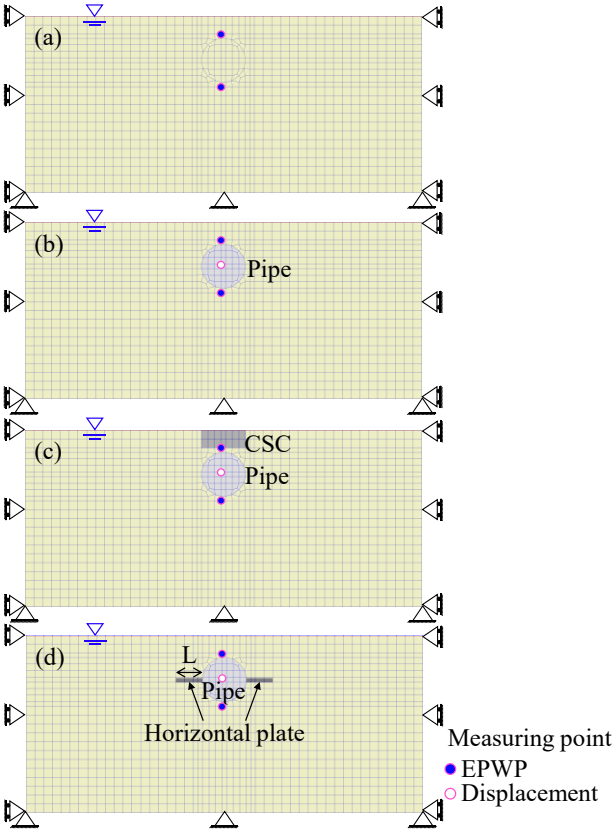

Figure 4. FE models and boundary conditions (a) homogeneous soil model, (b) NC pipe model, (c) CSC pipe model, and (d) DSC pipe model.

Table 3. Numerical analysis cases.

Case	Conditions	Note
Homogeneous	Drained	Comparison – NC
Homogeneous	Undrained	
NC 1	Drained	Comparison – CSC
NC 2	Undrained	Compraison – DSC
CSC 1		k_{CSC}=3.6×10^{-3} m/s
CSC 2	Drained	k_{CSC}=5.1×10^{-3} m/s
CSC 3		k_{CSC}=6.0×10^{-3} m/s
DSC 1		L/D=0.2
DSC 2		L/D=0.4
DSC 3	Undrained	L/D=0.6
DSC 4		L/D=0.8
DSC 5		L/D=1.0

4 RESULTS

4.1 Uplift displacement of pipe

Figure 5 and Figure 6 show the uplift displacement of pipes. The lower uplift in numerical analysis than experiment on NC pipe and CSC pipe model seems to be due to the limitation of the finite element method (FEM), in which the soil elements of the pipe's upper side remain without scattering during uplift. Except for that, validation seems to be done well under undrained conditions.

Figure 5 shows the NC pipe and CSC pipe uplift displacement. CSC showed a larger uplift than NC in both experiments and numerical analysis, and this increased as the CSC's permeability increased. This indicates that the high-permeable material at the top of the pipe is inducing more uplift.

Figure 6 shows NC pipe and DSC pipe uplift displacement. The DSC is analysed to be effective, and the tendency of pipe uplift to decrease rate decrease from the *L*/*D* equals to 0.6. Therefore, this study assumes that the *L*/*D* 0.6 is the most reasonable type.

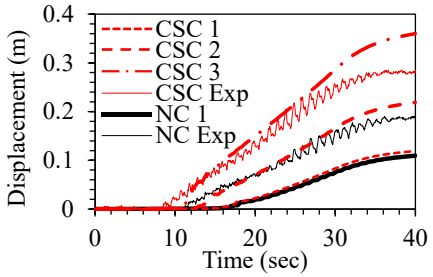

Figure 5. Uplift displacement of NC and CSC pipes.

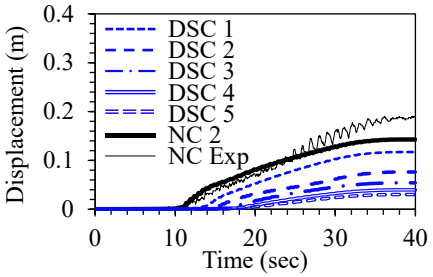

Figure 6. Uplift displacement of NC and DSC pipes.

4.2 Excess pore water pressure (EPWP)

Figure 7(a) shows the experimental EPWP at the pipe's upper side. EPWP initially accumulated due to shaking at the pipe's upper side, but as the pipe uplifted, it decreased due to the reduction in pore water pressure according to submerged depth. Applying CSC tends to reduce the increase in EPWP at the pipe's upper side. Figure 7(b) shows the experimental EPWP at the pipe's lower side. There was a rapid volume expansion at the pipe's lower side due to pipe uplift, which resulted in a negative EPWP. It is analysed that this negative EPWP increases the effective stress of the pipe's lower side soil and acts as a downward dragging force. It was observed that applying CSC recovered these negative EPWPs faster than NC.

Figures 8(a) and (b) show the EPWP at the pipe's upper and lower sides based on numerical analysis of drained conditions. EPWP behaviour of numerical analysis showed differences from experiments due to the measuring mechanism. The numerical analysis measures the EPWP at the fixed node of the soil element, but the experiment measures the EPWP through the sensors attached to the pipe. These sensors measure surrounding pore water pressure, not the EPWP of the soil, which experiences faster EPWP dissipation (pipe's top) a larger pressure change during uplift (pipe's bottom). However, similar to the experiment, numerical analysis shows that CSC is well dissipating the EPWP during the shaking.

However, larger pipe uplift displacements were shown in CSCs. This is analysed because CSC renders the uplift-prone pressure condition around the pipe. Specifically, based on the principle that fluid flows from the high-pressure side to a low-pressure side, CSC creates a lower-pressure condition than NC at the pipe's upper side and a higher-pressure condition than NC at the pipe's lower side.

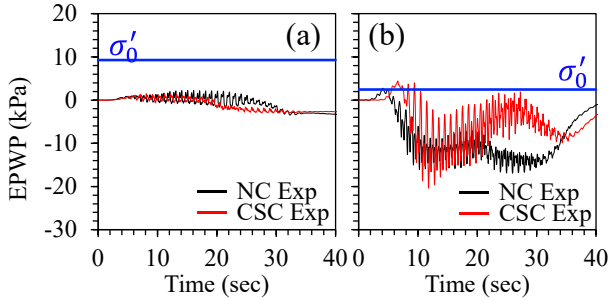

Figure 7. Excess pore water pressure (EPWP) according to the total time history (Experiment) (a) upper side of the pipe (P1, P2), (b) lower side of the pipe (P3, P4).

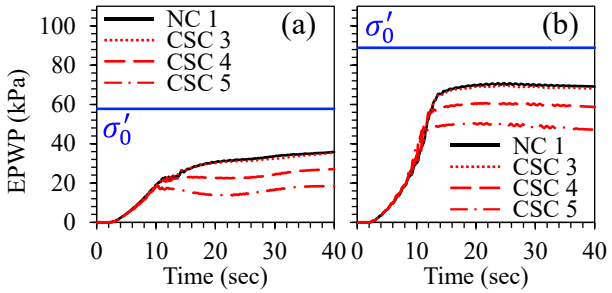

Figure 8. Excess pore water pressure (EPWP) according to the total time history (Numerical analysis) (a) upper side of the pipe, (b) lower side of the pipe.

Figure 9 shows the EPWP ratio at 10, 20, and 36-second points by input motion (Figure 2) of the homogeneous soil, NC pipe, and DSC (*L*/*D*=0.6) pipe

models based on numerical analysis of undrained conditions. It was judged more appropriate to analyse the liquefaction behaviour through overall images rather than EPWP at one point. In addition, due to the EPWP range difference caused by the different pipe conditions, a method of analysis through the EPWP ratio was adopted.

A comparison between the homogenous soil and the NC pipe models shows that the EPWP ratio increased slightly at the pipe's upper side soil at the 10-second point. This is analysed because the pipe uplift is applying additional pressure to the pipe's upper side soil. This mechanism has been verified with the drained conditions in a previous study (Hong et al., 2024). From the 20 seconds, the EPWP ratio reduction shows at the pipe's lower side due to the volume expansion of the pore water, and this EPWP reduction is analysed to perform as a significant pipe uplift resistance force. Consequently, the countermeasure design should focus on reducing the pipe uplift pressure in the pipe's upper side soil and increasing the volume expansion area in the pipe's lower side soil.

Comparison between the NC and DSC pipe models shows that the EPWP ratio decreases in the soil around the horizontal plate. This EPWP ratio decrease is noticeable at the lower side of the horizontal plate, and it is analysed due to the increased pipe uplift-induced volume expansion area. However, NC shows a lower EPWP ratio at the pipe bottom soil than the DSC. This is not because the NC pipe is well-resisting against uplift but because the NC pipe's larger uplift induces more volume expansion at its bottom. Therefore, excluding the decrease in EPWP ratio due to NC's larger uplift-induced volume expansion, DSC is effective by enhancing the uplift resistance generated in the soil below the pipe.

Furthermore, DSC increases the load on the upper soil by enlarging the soil volume above the horizontal plates. Therefore, the application of DSC can be seen as a countermeasure to not only mitigate EPWP build-up but also increase the pipe uplift resistance force caused by the upper soil. Since the effect of increasing the pipe's upper side soil load by DSC increases in deeper buried conditions, it is analysed that the effect will be greater in the actual field, which is usually deeper than this study's burial condition (H/D=1).

5 CONCLUSIONS

This study verified the various countermeasures' effectiveness in reducing the buried pipe uplift in liquefied ground. As a result of the experiment and numerical analysis on high-permeable countermeasure that is known as effective and numerical analysis on horizontal plate countermeasure that overcome the problems shown in existing rigid structure countermeasures, the main conclusions are as follows:

1) Although replacing the soil on the pipe's top with high-permeable material could reduce excess pore water pressure, it was confirmed that it could cause pipe uplift-prone pressure conditions. This suggests that the sole use of high-permeable materials may not necessarily be effective.
2) Through numerical analysis, the horizontal plate placing at the mid-height of the pipe effectively reduced pipe uplift by mitigating the EPWP build-up around the pipe and increasing the uplift resistance force by the pipe's upper side soil.

Further experiments on the horizontal plate countermeasure are needed to find specific and optimized application methods. The findings of this study are expected to contribute to earthquake-induced disaster prevention research on underground infrastructure uplift damage.

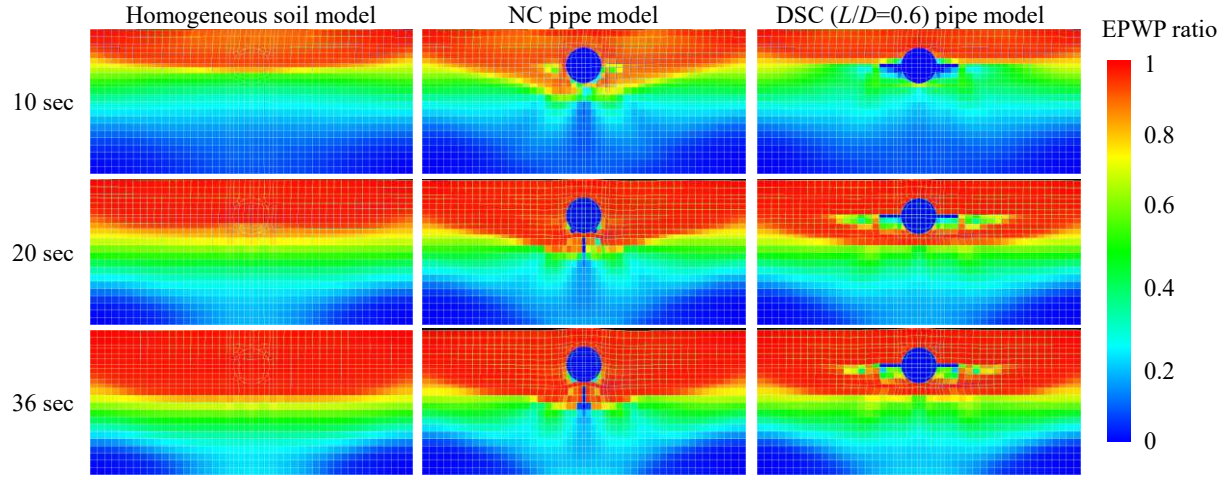

Figure 9. EPWP ratio according to the total time history.

ACKNOWLEDGEMENTS

This study is supported by the "Subcommittee on rational earthquake and tsunami countermeasures for water and sewage facilities" in the Japan Society of Civil Engineers earthquake engineering committee.

REFERENCES

Chian, S. C., Tokimatsu, K., and Madabhushi, S. P. G. (2014). Soil liquefaction–induced uplift of underground structures: physical and numerical modeling. *Journal of Geotechnical and Geoenvironmental Engineering*, 140(10), 04014057. https://doi.org/10.1061/(ASCE)GT.1943-5606.0001159

Chian, S. C. and Madabhushi, S. P. G. (2012). Effect of buried depth and diameter on uplift of underground structures in liquefied soils. *Soil Dynamics and Earthquake Engineering*, 41, 181-190. https://doi.org/10.1016/j.soildyn.2012.05.020

Sharafi, H. and Parsafar, P. (2016). Seismic simulation of liquefaction-induced uplift behavior of buried pipelines in shallow ground. *Arabian Journal of Geosciences*, 9, 1-9. https://doi.org/10.1007/s12517-015-2025-y

Basu, D. and Wijewickreme, D. (2024). Influence of ground motion characteristics on liquefaction-induced pipe uplift. *Japanese Geotechnical Society Special Publication*, 10(22), 838-842. https://doi.org/10.3208/jgssp.v10.OS-11-06

Castiglia, M., de Magistris, F. S., Onori, F., and Koseki, J. (2021). Mitigation systems for the uplift of buried pipelines in liquefiable soils under repeated shaking through model tests. *Soil Dynamics and Earthquake Engineering*, 148, 106850. https://doi.org/10.1016/j.soildyn.2021.106850

Valizadeh, H. and Ecemis, N. (2022). Soil liquefaction-induced uplift of buried pipes in sand-granulated-rubber mixture: Numerical modeling. *Transportation Geotechnics*, 33, 100719. https://doi.org/10.1016/j.trgeo.2022.100719

Ecemis, N., Valizadeh, H., and Karaman, M. (2021). Sand-granulated rubber mixture to prevent liquefaction-induced uplift of buried pipes: a shaking table study. *Bulletin of Earthquake Engineering*, 19, 2817-2838. https://doi.org/10.1007/s10518-021-01091-3

Hong, H., Tobita, T., Katsutoshi, M., and Yasuhiko, K. (2024). Analysis of resistance mechanisms and countermeasures against pipe uplift during liquefaction. *Japanese Geotechnical Society Special Publication*, 10(51), 1912-1917. https://doi.org/10.3208/jgssp.v10.OS-40-03

Taeseri, D., Laue, J., Otsubo, M., and Towhata, I. (2016). New mitigation method for pipeline uplift during seismic event. *Geotechnical Research*, 3(2), 54-64. https://doi.org/10.1680/jgere.16.00002

Madabhushi, G. (2017). *Centrifuge modelling for civil engineers*. CRC press. https://doi.org/10.1201/9781315272863

Ueno. S., Sasaoka. N., Mori. K., Nakamura. K., Fukushima. M., and Suwa. Y., (2017). Analysis of soil conditions related to piping development on river embankments based on model experiments. *Collection of river technology papers*, 23, 405-410. (Japanese) https://doi.org/10.11532/river.23.0_405

Asano. I., Hayashida. Y., Masukawa. S., and Tazumi. H. (2010). Relationship between flow velocity and hydraulic gradient of flow passing through porous concrete. *Agricultural Research and Development Bulletin*, 210, 227-241 (Japanese)

Mori, A. and Tamura, M. (1986). Effect of dilatancy on permeability in sands stabilized by chemical grout. *Soils and Foundations*, 26(1), 96-104. https://doi.org/10.3208/sandf1972.26.96

Inoue. K., Yamada. M., Domyo. Y. (2019). Influence of Relative Density of Sand on Permeability Coefficient —Constant Head Permeability Test Results of Three Types of Sand— *Nihon University College of Science and Technology Academic Lecture Proceedings* B-68 (Japanese)

Iai, S., Tobita, T., Ozutsumi, O., and Ueda, K. (2011). Dilatancy of granular materials in a strain space multiple mechanism model. *International Journal for Numerical and Analytical Methods in Geomechanics*, 35(3), 360-392. https://doi.org/10.1002/nag.899

Asadi, M. B., Orense, R. P., Asadi, M. S., & Pender, M. J. (2019). Liquefaction assessment of pumiceous sand with shear wave velocity approach. In Earthquake Geotechnical Engineering for Protection and Development of Environment and Constructions (pp. 1186-1193). CRC Press. https://doi.org/10.1201/9780429031274

Zienkiewicz, O. C., Chang, C. T., and Bettess, P. (1980). Drained, undrained, consolidating and dynamic behaviour assumptions in soils. *Geotechnique*, 30(4), 385-395. https://doi.org/10.1680/geot.1980.30.4.385